Joint Trajectory and Velocity-Time Optimization for Throughput Maximization in Energy-Constrained UAV

Nishant Gupta, *Student Member, IEEE*, Satyam Agarwal, *Member, IEEE*, and Deepak Mishra, *Member, IEEE*

***Abstract*—In this article, we aim to study an unmanned aerial vehicle (UAV)-assisted Internet of Things (IoT) communication system where a rotary-wing UAV travels from the initial to the final location to communicate with multiple IoT ground devices. The limited onboard energy of the UAV poses a constraint to the overall system's performance. UAV's energy consumption is majorly based on its kinematics, i.e., UAV's velocity and acceleration. Therefore, in this work, we maximize the sum user throughput by jointly optimizing the 3-D UAV trajectory, and velocity-time profile in the presence of onboard energy, velocity, acceleration, and completion time constraints. Noting the nonconvexity of the optimization problem, the original problem is decoupled into two subproblems. First, the trajectory is optimized considering the velocity constraint, while in the second subproblem, the velocity and time optimization in each time slot is carried out. Simulation results show insights on the UAV trajectory and velocity-time profile with the variation in the onboard energy availability. In addition, we demonstrate the superior performance of the proposed approach in comparison to the benchmark schemes.**

***Index Terms*—Energy constraint, 3-D trajectory, unmanned aerial vehicle (UAV)-enabled Internet of Things (IoT) communication, velocity and time optimization.**

I. Introduction

THE Internet of Things (IoT) has emerged as a technological revolution that promotes the current age of pervasive connection, computation, and communication [1]. However, the exponential growth in the demand for data transmission in IoT creates a significant challenge [2]. Thus, in IoTs, the use of unmanned aerial vehicles (UAVs) from an application perspective is becoming a very prominent and promising technology due to their extensive features, such as wide coverage, high mobility, and on-demand deployment [3]. Nowadays, the use of UAVs as a mobile aerial access point (AP) is becoming very popular to improve the system's throughput and provide seamless connectivity to the IoT ground devices (GDs) [4].

In a UAV-enabled IoT network, the UAV can either collect from or disseminate information to the IoT GDs. Thus, to achieve better performance, the throughput of the system needs to be maximized [5]. However, UAV operations pose serious challenge in terms of its available onboard energy. As a result, the overall lifespan of the communication service provided by the UAV is limited. The onboard energy available with the UAV is utilized in manoeuvring which is determined by its flying velocity-acceleration profile and flight time. Thus, the communication system's design must consider energy consumption as a function of UAV velocity, acceleration, and time along with the other constraints.

In this context, this article considers an appropriate UAV-enabled IoT network that jointly optimizes 3-D UAV trajectory, velocity, and time to maximize the sum user throughput while considering the UAV kinematics (velocity and acceleration), mission completing time, and UAV energy consumption as a function of velocity and acceleration as constraints. The rotary-wing UAV is considered in this work due to its appealing advantages, such as ability to hover at a fixed location and take-off vertically [6]. The proposed problem is challenging since it includes multiple nonconvex functions, such as onboard energy, user throughput, etc. Also, the nonlinear relationship between the 3-D UAV trajectory and energy consumption as described in [7] also makes the problem nontrivial to deal with. Therefore, this article is devoted to maximize the sum throughput with a limited energy budget, subject to the constraints on the UAV velocity, acceleration, and flight duration in traveling from the initial to the final location.

A. Related Work

With the aim to maximize system throughput, UAV trajectory and resource allocation were jointly optimized in [8], and [9]. The throughput of the UAV-enabled mobile relaying system was considered in [10] to optimize the UAV trajectory and transmit power allocation under various realistic limitations. You and Zhang [11], [12] maximized the minimum expected data rate in probabilistic Line-of-Sight (LoS) channels and Rician fading, respectively, to investigate the 3-D trajectory and communication scheduling. Lu *et al.* [13] considered a secure communication scheme, where the 2-D trajectory and

Manuscript received 21 May 2022; accepted 1 July 2022. Date of publication 11 July 2022; date of current version 21 November 2022. This work was supported in part by the Department of Science and Technology under Grant DST/INSPIRE/04/2016/001127 and Grant CRG/2020/005749, and in part by IIT Ropar ISIRD Grant under Grant 9-362/2018/IITRPR/1590. *(Corresponding author: Nishant Gupta.)*

Nishant Gupta and Satyam Agarwal are with the Department of Electrical Engineering, Indian Institute of Technology Ropar, Rupnagar 140001, India (e-mail: 2018eez0018@iitrpr.ac.in; satyam@iitrpr.ac.in).

Deepak Mishra is with the School of Electrical Engineering and Telecommunications, University of New South Wales, Sydney, NSW 2052, Australia (e-mail: d.mishra@unsw.edu.au).

Digital Object Identifier 10.1109/JIOT.2022.3189689

2327-4662 © 2022 IEEE. Personal use is permitted, but republication/redistribution requires IEEE permission.
See https://www.ieee.org/publications/rights/index.html for more information.

Authorized licensed use limited to: Beijing Information Science & Tech Univ. Downloaded on March 19,2023 at 02:57:14 UTC from IEEE Xplore. Restrictions apply.

resource allocation are optimized to maximize the minimum secure capacity. In [14], the throughput maximization problem was investigated, where the 3-D UAV trajectory and resource allocation were studied while considering constraints on energy harvesting. Note that we have not considered the works that include the UAV trajectory optimization where the UAV flies at a fixed altitude, for example, [15] and [16]. Despite the fact that these efforts have substantially increased the throughput of the communication system, the limited energy availability of UAV was not considered. This issue is important because the limited UAV's onboard energy restricts the trajectory and limits the coverage duration, causing the UAV to provide short-term communication service instead of a long-term continuous communication.

Keeping in view the on-board energy availability, several works that have considered the on-board energy consumption as a function of UAV velocity and acceleration are [17]–[21]. In the above works, the authors have either maximized the energy efficiency or minimized the energy consumption while considering a fixed-wing UAV. Furthermore, the analysis provided for fixed-wing UAVs can not be extended to the rotary-wing UAVs due to their fundamentally different mechanical designs. In general, the fixed-wing UAV requires less energy while flying at nominal speeds and a tremendous amount of energy while flying at lower speeds; moreover, they cannot hover at a particular location. On the other hand, the rotary-wing UAVs consume lesser finite energy than the fixed-wing UAVs when hovering or flying at lower speeds. Therefore, such solutions to obtain the trajectory of the fixed-wing UAV do not apply to our considered scenarios.

To this extent, the works in [7] and [22] derived a velocity-acceleration dependent energy consumption model of a rotary-wing UAV. In particular, Yang *et al.* [7] minimized the energy consumption of the UAV while assuming the UAV to fly in a single dimension only.

From the communication perspective, several works [23]–[30] have considered the energy consumption as a constraint in their works. In particular, Nguyen and Le [23] maximized the overall throughput of the system while considering velocity-independent energy consumption. Eom *et al.* [24] and Jing *et al.* [25] considered the velocity-acceleration dependent energy consumption model but for a fixed-wing UAV and considered the UAV-user channel model dominated by LoS links. Similarly, Hu *et al.* [26] considered the velocity-acceleration profile but for a fixed-wing UAV and a segmented ray-tracing UAV-user channel model. For the probabilistic-LoS channel model, Zhang *et al.* [27] maximized the system's throughput and considered the UAV to travel with the fixed/constant velocity and assumed that the energy consumed by the UAV in each time slot is equal to the sleep energy of the UAV. Similarly, Wu *et al.* [28] and Gupta *et al.* [29] minimized the cost/energy of the UAV and the system's throughput, respectively, while assuming the UAV to move with a constant velocity such that the energy consumed in every time slot is fixed. Meng *et al.* [30] maximized the throughput of the system by taking an approximate probabilistic LoS channel model and velocity-dependent energy consumption model for a rotary-wing UAV.

In general, the propulsion energy consumption model of a rotary-wing UAV depends upon its mobility. Many prior works have considered either the fixed velocity of the UAV throughout its flight or they do not account for acceleration-dependent energy consumption. UAV acceleration results in a significant amount of energy consumption and plays a critical role in designing an optimal UAV trajectory (Section II-C). To the best of author's knowledge, the aforementioned energy model has not been considered in the prior works. Therefore, in this article, we consider velocity and acceleration dependent energy consumption model of a UAV and jointly optimize the UAV trajectory and velocity-time profile to maximize the sum throughput of all users. We also consider a practical channel model that comprises of LoS and non-LoS (NLoS) links along with their certain occurrence probabilities. To show the key differences of our work with the prior art, we have added a summary table in Table I. It can be verified from the table that our work is the first work that studies the velocity-acceleration and time profile under a practical channel model while considering the energy model for a rotary-wing UAV.

B. Motivation and Contributions

In this article, we develop a framework where a rotary-wing UAV is dispatched from the initial location to communicate with multiple IoT GDs. Such a setup can be applied to various practical applications, including UAV-enabled data collection, information dissemination, UAV-enabled caching [31], etc. Our objective is to design a 3-D trajectory of the UAV along with determining its suboptimal velocity-acceleration and time profile to maximize the system-level goal like sum throughput, including the UAV practical constraints.

The main contributions of this article are as follows.

1) Since the velocity and acceleration play a critical role in the energy consumption of the UAV, in this article, we consider a velocity-acceleration dependent energy consumption model of a rotary-wing UAV. Considering this energy model, we develop an optimization framework to jointly optimize the 3-D UAV trajectory, velocity-acceleration, and time profile to maximize the sum throughput.
2) We propose a solution strategy that decomposes the original framework into two subproblems. First, optimizes the UAV trajectory by considering the velocity constraint and relaxing the acceleration and onboard energy constraints. Second, utilizes this solution to optimize the velocity and time to improve the sum throughput performance of the obtained trajectory.
3) Noting the nonconvexity of the above subproblems, an iterative approach based on successive convex approximation (SCA) and alternating optimization is presented to obtain the solution of the first subproblem. For the second subproblem, we first transform the problem and then apply SCA to solve it.
4) We present a low-complexity iterative approach that obtains the UAV trajectory and velocity-time profile while considering the onboard energy availability.

Authorized licensed use limited to: Beijing Information Science & Tech Univ. Downloaded on March 19,2023 at 02:57:14 UTC from IEEE Xplore. Restrictions apply.

TABLE I
KEY DIFFERENCES BETWEEN THE RELATED EXISTING LITERATURE WITH OUR WORK. PLOS HERE STANDS FOR PROBABILISTIC LOS CHANNEL

Ref.	Objective	Velocity profile	Acceleration profile	Time profile	Channel model	Scenario considered	Energy consumption model
[23]	Maximize throughput	✓	×	✓	LoS	2D	Approximated model
[24]	Max-min Rate	✓	✓	×	LoS	2D	Fixed-wing UAV
[25]	Maximize coverage to number of ground users	✓	✓	✓	LoS	2D	Fixed-wing UAV
[26]	Max-min Throughput	✓	✓	×	Segmented Ray-tracing model	3D	Fixed-wing UAV
[27]	Maximize throughput	Fixed	×	✓	PLoS	2D	Fixed energy
[28]	Minimize cost/energy of UAV	Constant speed	×	×	PLoS	2D	Velocity-dependent
[29]	Maximize throughput	Fixed-maximum speed	×	✓	PLoS	3D	Maximum-velocity
[30]	Maximize throughput	✓	×	×	Approximate PLoS	3D	Velocity-dependent
Ours	Maximize throughput	✓	✓	✓	PLoS	3D	Rotary-wing UAV

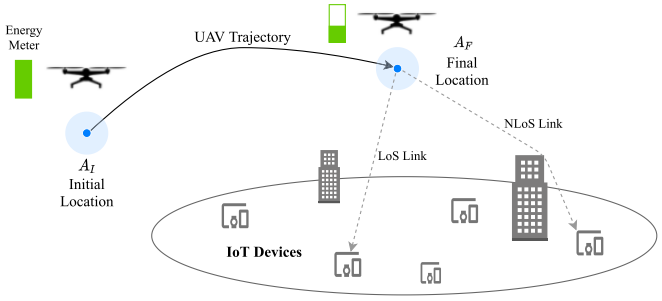

Fig. 1. System model for UAV-enabled IoT communication system.

Furthermore, we also provide the complexity analysis of the iterative approach.

5) Finally, we conduct extensive simulations to evaluate the performance of our proposed 3-D UAV trajectory. We show how the overall energy consumption constraint impacts the velocity, acceleration, and time profile in each time slot and compare the system's performance with the existing benchmark schemes.

The organization of this article is as follows. Section II describes the system and channel model for the UAV-enabled IoT communication system. Section III defines the problem statement along with the proposed solution methodology. The mathematical formulations and algorithm designs of both the subproblems are described in Sections IV and V. The overall algorithm implementation and its complexity analysis is described in Section VI. Numerical results and discussions are provided in Section VII, and finally, this article is concluded in Section VIII.

II. SYSTEM MODEL

A UAV-enabled IoT communication system as shown in Fig. 1 is considered, where a rotary-wing UAV is used to provide communication in a circular field with N IoT GDs. The GDs are represented by a set $\mathcal{N} = \{1, \ldots, N\}$. The location of the nth-GD is fixed and is given by $[x_n^g, y_n^g] \in \mathbb{R}^{1\times 2} \quad \forall n \in \mathcal{N}$, where $\mathbb{R}$ denotes the real-valued number set. The UAV is launched from the initial location A_I with coordinates (x^I, y^I, z^I) and moves to the final location A_F with coordinates (x^F, y^F, z^F). Moreover, the transition of UAV from the initial to the final location is subjected to some practical constraints, such as velocity, acceleration, onboard energy availability, etc.

A. UAV Trajectory Model

For ease of analysis, the total completion time available with the UAV to reach from the initial to the final location is divided into M slots, indexed by $\mathcal{M} = \{0, 1, \ldots, M\}$ and the mth-slot is of duration $\tau[m]$, where $m \in \mathcal{M}$. The time slot duration is chosen such that the distance traveled by the UAV in a time slot is much smaller than the distance between the UAV and the GDs [32]. The UAV moves from the initial location A_I to the final location A_F in M slots and the UAV position in the mth-time slot is $(x^u[m], y^u[m], z^u[m])$, where $m = 0$ implies the UAV is at the initial location and $m = M$ implies the UAV is at the final location. We assume that in the mth-time slot, the UAV moves with a fixed acceleration $a[m]$ (m/s^2) and the velocity achieved by the UAV at the end of the mth-time slot is $v[m]$ (m/s). For all quantitative consideration, we consider the location of the UAV at the end of a given time slot to be the UAV location in that time slot. Similarly, the UAV velocity at the end of the time slot is considered to be the velocity of the UAV in that slot for ease of analysis. This hold when $\tau[m]$ is sufficiently small.

To avoid obstacles/building, etc., we ensure that the UAV makes lateral movement only when its height is above a minimum threshold height $H_{\min}$, i.e., the UAV only makes vertical movement when its height is below $H_{\min}$. Apart from this, the UAV velocity and acceleration is restricted to a maximum velocity $V_{\max}$ and acceleration $A_{\max}$ obtainable by the UAV. The total time of the UAV to transit from the initial to the final location is also restricted to $T_{\max}$.

B. Channel Model

We consider that the UAV communicates with GDs over a communication channel with bandwidth B (Hz). It uses frequency division multiple access (FDMA) to equally share the available resource amongst the GDs. UAV's being different from terrestrial transceivers experience better LoS links, and its UAV-GD link mainly depends upon the elevation angle and the type of propagation environment. Thus, a probabilistic LoS channel model is considered, where the UAV-GD link

Authorized licensed use limited to: Beijing Information Science & Tech Univ. Downloaded on March 19,2023 at 02:57:14 UTC from IEEE Xplore. Restrictions apply.

can experience either LoS or NLoS based on certain occurrence probabilities [33]. This LoS occurrence probability can be expressed in terms of a Sigmoidal function given as

$$P_{\text{LoS}}(\phi_n[m]) = \frac{1}{1 + C\exp(-D[\phi_n[m] - C])} \tag{1}$$

where C and D are environment dependent parameters, wherein the environment can be suburban, urban, dense urban, etc. $\phi_n[m]$ is the elevation angle (in degrees) of the UAV from the nth-GD at mth-time slot and is given by $\phi_n[m] = (180/\pi)\sin^{-1}(z^u[m]/d_n[m])$. Here, $d_n[m]$ is defined as the distance between the nth-GD and the UAV at the mth-time slot, and is given as $d_n[m] = \sqrt{(z^u[m])^2 + \|(x^u[m], y^u[m]) - (x_n^g, y_n^g)\|^2} \quad \forall n \in \mathcal{N} \quad \forall m \in \{1, \ldots, M\}$, where $\|.\|$ is the norm operator.

Taking into account the large-scale fading effects (h_n^l) and small-scale fading effects (h_n^s) for UAV-GD link, the channel model for nth-GD at mth-time slot is given by $H_n[m] = h_n^l[m]h_n^s[m]$. The large-scale fading effects for both LoS and NLoS links are expressed as $|h_n^l[m]|^2 = \beta_0 d_n[m]^{-\bar{\alpha}}$, for LoS link, and $|h_n^l[m]|^2 = \kappa\beta_0 d_n[m]^{-\bar{\alpha}}$, for NLoS link, where β_0 represents the pathloss at a reference distance, $\bar{\alpha}$ represents the pathloss exponent, and $\kappa < 1$ accounts for the additional attenuation factor [6, eq. (2)].

Since the small-scale fading coefficient is independent of the large-scale fading coefficient, using the property of small-scale fading, i.e., $\mathbb{E}[|h_n^s[m]|^2] = 1$, [6], then, $\mathbb{E}[|H_n[m]|^2]$ can be expressed as follows:

$$\begin{aligned}\mathbb{E}\Big[|H_n[m]|^2\Big] &= P_{\text{LoS}}(\phi_n[m])\beta_0 d_n[m]^{-\bar{\alpha}} + (1 - P_{\text{LoS}}(\phi_n[m])) \\ &\quad \times \kappa\beta_0 d_n[m]^{-\bar{\alpha}} \\ &= \widehat{P}_{\text{LoS}}(\phi_n[m])\beta_0 d_n[m]^{-\bar{\alpha}}\end{aligned} \tag{2}$$

where $\widehat{P}_{\text{LoS}}(\phi_n[m]) = (1 - \kappa)P_{\text{LoS}}(\phi_n[m]) + \kappa$.

Let P_{tr} denote the UAV transmit power. The average received signal-to-noise (SNR) γ is given by

$$\mathbb{E}\big[\gamma_n[m]\big] = \mathbb{E}\left[\frac{P_{tr}|H_n[m]|^2}{\sigma^2}\right] = \frac{P_{tr}\mathbb{E}\big[|H_n[m]|^2\big]}{\sigma^2} \tag{3}$$

where σ^2 is the channel noise power at the receiver. Then, the overall expected throughput in bits-per-second (bps) of the nth-GD at mth-time slot is given by

$$r_n[m] \approx \frac{B}{N}\log_2\left(1 + \frac{P_{tr}\mathbb{E}\big[|H_n[m]|^2\big]}{\sigma^2}\right). \tag{4}$$

Then, the overall sum throughput $\mathcal{R}$ averaged over time of the UAV-enabled IoT communication system is given by

$$\mathcal{R} = \frac{\sum_{m=1}^{M}\sum_{n=1}^{N}\tau[m]r_n[m]}{\sum_{m=1}^{M}\tau[m]}. \tag{5}$$

C. UAV Energy Consumption Model

In general, UAV energy consumption consists of propulsion energy and communication-related energy. It has been shown in [34] that the communication energy is far less than the propulsion energy. Therefore, in this article, we mainly focus on propulsion energy. As discussed in [7], the propulsion energy consumption comprises of two components: 1) energy consumption during level-straight flight and 2) energy consumption in vertical flight. Moreover, for simplicity, we have utilized the same energy model as derived in [7] to design the UAV trajectory in this work. Accordingly, the UAV velocity $v[m]$ in a time slot can be decomposed into two components, namely, the horizontal and the vertical components denoted by $v^{xy}[m]$ and $v^z[m]$, respectively. Similarly, the UAV acceleration $a[m]$ in a time slot can be decomposed into horizontal and vertical components and is given as $a^{xy}[m]$ and $a^z[m]$, respectively. The relation between UAV velocity and acceleration is expressed as follows:

$$v^{xy}[m] = \frac{2\|(x^u[m], y^u[m]) - (x^u[m-1], y^u[m-1])\|}{\tau[m]} - v^{xy}[m-1] \tag{8}$$

$$v^z[m] = \frac{2(z^u[m] - z^u[m-1])}{\tau[m]} - v^z[m-1] \tag{9}$$

$$a^{xy}[m] = \frac{v^{xy}[m] - v^{xy}[m-1]}{\tau[m]} \tag{10}$$

$$a^z[m] = \frac{v^z[m] - v^z[m-1]}{\tau[m]} \tag{11}$$

where these equations represent the mathematical relationship between the UAV displacement in the mth-time slot, UAV's velocities at the mth and the $(m-1)$th-time slot, and time duration of mth-time slot for the horizontal and vertical components, respectively. Note that the overall velocity in a time slot is the resultant of the horizontal and vertical component i.e., $v[m] = \sqrt{(v^{xy}[m])^2 + (v^z[m])^2}$, and similarly, $a[m] = \sqrt{(a^{xy}[m])^2 + (a^z[m])^2}$.

Then, as defined in [7], the propulsion energy consumption of a rotary-wing UAV under individual horizontal and vertical components for the mth-time slot is given by $e^{xy}[m]$ and $e^z[m]$, shown in (6) and (7), at the bottom of the page, respectively. Here, P_0, P_1, P_2, C_1, C_2, C_3, C_4,

$$e^{xy}[m] = \tau[m]\Bigg(P_0\Big(1 + C_1\big(v^{xy}[m]\big)^2\Big) + P_1\sqrt{1 + \big(C_2(v^{xy}[m])^2 + C_3 a^{xy}[m]v^{xy}[m]\big)^2}\Bigg) \cdot \sqrt{\sqrt{1 + \big(C_2(v^{xy}[m])^2 + C_3 a^{xy}[m]v^{xy}[m]\big)^2 + C_4^2(v^{xy}[m])^4} - C_4(v^{xy}[m])^2 + C_5\big(v^{xy}[m]\big)^3}\Bigg) \tag{6}$$

$$e^z[m] = \tau[m]\left(P_2 + \frac{W_{en}v^z[m] + M_{en}a^z[m]v^z[m]}{2} + \frac{W_{en} + M_{en}a^z[m]}{2}\sqrt{(v^z[m])^2 + \frac{2(W_{en} + M_{en}a^z[m])}{\rho A_{en}}}\right) \tag{7}$$

Authorized licensed use limited to: Beijing Information Science & Tech Univ. Downloaded on March 19,2023 at 02:57:14 UTC from IEEE Xplore. Restrictions apply.

TABLE II
ENERGY CONSUMPTION MODEL PARAMETERS

Parameter	Symbol	Value
Profile drag coefficient	δ	0.012
Air density (kg/m^3)	ρ	1.225
Rotor solidity	ψ	0.05
Blade angular velocity (radians/second)	Ω	300
Rotor disc area (m^2)	A_{en}	0.503
Rotor radius (m)	R_{en}	0.4
UAV mass (kg)	M_{en}	2.04
Incremental correction factor to induced power	K_{en}	0.1
UAV weight (Newton)	W_{en}	20
Fuselage equivalent flat plate area (m^2)	S_{en}	0.0151
Fuselage drag ratio	D_{en}	0.6

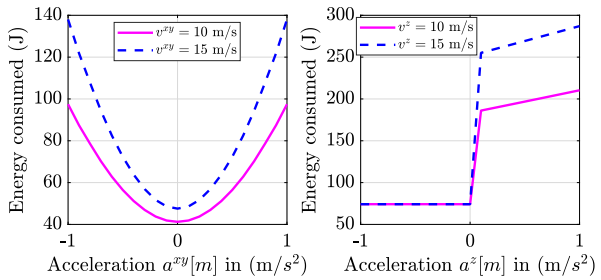

Fig. 2. Energy consumed with different accelerations for (a) level-straight flight and (b) vertical flight of UAV.

and C_5 are the constants whose values depend upon the mechanical parameters of the UAV and is given as $P_0 = (\delta/8)\rho\psi A_{en}\Omega^3 R_{en}^3$, $P_1 = (1+K_{en})[(W_{en}^{3/2})/(\sqrt{2\rho A_{en}})]$, $P_2 = P_0 + K_{en}([W_{en}^{3/2}]/[\sqrt{2\rho A_{en}}])$, $C_1 = (3/\Omega^2 R_{en}^2)$, $C_2 = (\rho S_{en}/2W_{en})$, $C_3 = (M_{en}/W_{en})$, $C_4 = (\rho A_{en}/W_{en})$, and $C_5 = (1/2)D_{en}\rho\psi A_{en}$, where the notations and physical meaning of the variables are given in Table II.

From the UAV mechanics, we know that the forward thrust is proportional to the mass of the UAV multiplied by the rate of change in velocity (acceleration) of the UAV. To show that the acceleration plays a crucial role in the UAV trajectory design, we present the UAV energy consumption with the variation in acceleration in Fig. 2. Fig. 2(a) and (b) shows the level-straight and vertical flight energy consumption, respectively. From Fig. 2, it can be observed that as the acceleration increases, the energy consumption significantly increases for a fixed velocity. Therefore, we need to consider the acceleration of the UAV along with the UAV velocity to design an energy-aware UAV trajectory.

Considering the propulsion energy of horizontal and vertical components, the total energy consumed by the UAV during its flight mission is given by

$$\mathcal{E}_{tot} = \sum_{m=1}^{M} e^{xy}[m] + \sum_{m=1}^{M} e^{z}[m]. \tag{12}$$

From (6), (7), and (12), it can be observed that the UAV propulsion energy consumption is a nonlinear function of UAV velocity and acceleration. Motivated by this, this article studies the suboptimal trajectory and varies the velocity, acceleration, and time of each time slot to meet the energy requirements. Assuming that the UAV has a maximum onboard energy $E_{\max}$, then the UAV energy constraint is given by $\mathcal{E}_{\text{tot}} \leq E_{\max}$.

III. PROBLEM DEFINITION

A. Problem Formulation

Our objective in this work is to maximize the overall sum throughput $\mathcal{R}$ of the system by obtaining a suboptimal UAV trajectory and velocity-time profile in going from the initial to the final location in the presence of velocity, acceleration, energy, and time constraints. Then, the UAV trajectory optimization problem is formulated as follows:

$$\text{(P1)}: \max_{\substack{\tau[m],\{x^u[m],y^u[m],z^u[m]\} \\ \forall m\in\{1,\ldots,M\}}} \mathcal{R} = \frac{\sum_{m=1}^{M}\sum_{n=1}^{N}\tau[m]r_n[m]}{\sum_{m=1}^{M}\tau[m]}$$

$$\text{s.t.} \quad \left(x^u[0], y^u[0], z^u[0]\right) = \left(x^I, y^I, z^I\right) \tag{13a}$$

$$\left(x^u[M], y^u[M], z^u[M]\right) = \left(x^F, y^F, z^F\right) \tag{13b}$$

$$z^u[m] \geq H_{\min} \quad \forall m \in \{1,\ldots,M-1\} \tag{13c}$$

$$v[m] \leq V_{\max} \quad \forall m \in \mathcal{M} \tag{13d}$$

$$|a[m]| \leq A_{\max} \quad \forall m \in \mathcal{M} \tag{13e}$$

$$\mathcal{E}_{\text{tot}} \leq E_{\max} \tag{13f}$$

$$\sum_{m=1}^{M} \tau[m] = T_{\max} \tag{13g}$$

where (13a) and (13b) represent the initial and the final location constraints, respectively. Equation (13c) represents the minimum altitude constraint. Equation (13d) represents the maximum velocity constraint, where $V_{\max}$ denotes the maximal velocity that a UAV can attain. $A_{\max}$ in (13e) denotes the maximum acceleration that a UAV can take. Also, due to the stringent battery life of the UAV, we have added an onboard energy constraint in (13f) such that the UAV reaches the final location before exhausting its full energy. Finally, $T_{\max}$ in (13g) denotes the total flight time of the UAV.

B. Proposed Solution Methodology

The formulated problem (P1) is nonconvex due to the following reasons. First, the presence of a nonconcave objective function that depends upon the UAV location $x^u[m]$, $y^u[m]$, and $z^u[m]$ not only via a distance function but also via probability of LoS, $P_{\text{LoS}}(\phi_n[m])$ defined in (1). Second, the energy constraint in (13f) is nonconvex. Thus, the optimization problem (P1) is difficult to solve using the basic convex optimization techniques.

To facilitate a computationally tractable solution, we propose a low complexity suboptimal solution. In this approach, we divide the trajectory optimization problem (P1) into two subproblems and then solve them iteratively to obtain a suboptimal solution of (P1). A brief description on the decoupling of problem (P1) is shown in Fig. 3. Subproblem 1 (SP1) described in Section IV, we optimize the UAV trajectory while constraining the UAV velocity and relaxing the constraints on acceleration and energy availability to maximize the objective function $\mathcal{R}$. Subproblem 2 (SP2) described in Section V aims to optimize the velocity and time duration of the UAV in each time slot for the obtained trajectory in SP1.

Authorized licensed use limited to: Beijing Information Science & Tech Univ. Downloaded on March 19,2023 at 02:57:14 UTC from IEEE Xplore. Restrictions apply.

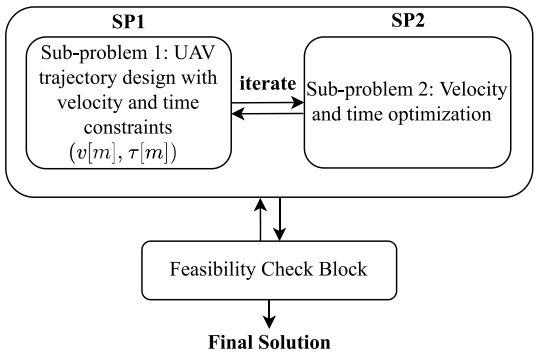

Fig. 3. Flowchart of the proposed solution to problem (P1).

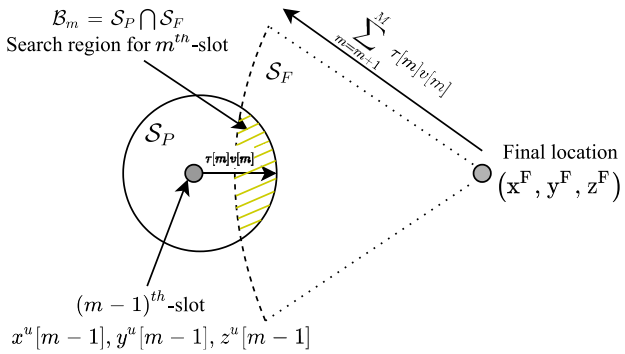

Fig. 4. Feasible search region for mth-time slot.

Subproblems SP1 and SP2 are solved iteratively using the alternating optimization method to obtain the joint trajectory and velocity-time profile. The final solution obtained from the alternating optimization method is then passed through the feasibility check block to verify the feasibility of the solution in terms of energy consumption constraint. If the solution is feasible, then this is the final solution. Otherwise, SP1 and SP2 are re-executed to obtain a better trajectory. Since, energy consumption decreases with a decrease in velocity, then to iterate the solution of SP1, we use velocity as a control variable. In this way, we iterate the subproblems until a feasible solution of (P1) is obtained.

IV. SP1: UAV Trajectory Optimization

A. Mathematical Formulation

In this subproblem SP1, we relax the acceleration (13e) and energy availability (13f) constraints in (P1) and constrain the UAV velocity. Accordingly the objective function $\mathcal{R}$ in (P1) is transformed into $\mathcal{R}_{\text{SP1}}^{\text{sum}} \triangleq \sum_{m=1}^{M}\sum_{n=1}^{N} \tau[m] r_n[m]$. The optimization problem SP1 is defined as follows:

$$\text{SP1:} \max_{\substack{\{x^u[m], y^u[m], z^u[m]\} \\ \forall\, m \in \{1,\ldots,M\}}} \mathcal{R}_{\text{SP1}}^{\text{sum}} \triangleq \sum_{m=1}^{M}\sum_{n=1}^{N} \tau[m] r_n[m]$$

$$\text{s.t.} \quad (13a),\ (13b),\ (13c)$$

$$\left\| \left(x^u[m], y^u[m], z^u[m]\right) - \left(x^u[m-1], y^u[m-1], z^u[m-1]\right) \right\| \leq \tau[m] v[m] \quad \forall m \in \mathcal{M} \tag{14a}$$

where (14a) represents the velocity constraint with $v[m]$ and $\tau[m]$ being the velocity of the UAV in each time slot and time slot duration, respectively. Since subproblem SP1 is called multiple times as discussed in Section III-B, $v[m]$ is set as a control variable whose value is always less than or equal to $V_{\max}$.

Problem SP1 is nonconvex where nonconvexity arises from the objective function with respect to UAV trajectory $(x^u[m], y^u[m], z^u[m])$. To find the solution to SP1, we proceed via finding the UAV location in each time slot while achieving maximum throughput over all users until the UAV reaches the final location as described in the next section. This sum throughput over all users in the mth-time slot is given by, i.e., $\mathcal{R}_{\text{SP1}}[m] = \sum_{n=1}^{N} r_n[m]$.

B. UAV Location in Each Time Slot

From (14a), we know that the distance traveled by the UAV in each time slot is bounded by $\tau[m]v[m]$. Thus, to find the optimal location in a time slot, we need to search inside a sphere of radius $\tau[m]v[m]$, centered at the UAV's previous location. As the UAV has to reach to the final location within M time slots, the search region can be reduced even further. This is done by using the geometric techniques, where we construct two spheres. One from the previous slot's location, i.e., $(m-1)$th-slot with radius $\tau[m]v[m]$, denoted by $\mathcal{S}_P$, specifying the region where the UAV can fly in a single time slot. The other sphere with radius $\sum_{m=m+1}^{M} \tau[m]v[m]$, denoted by $\mathcal{S}_F$, is built from the final location (x^F, y^F, z^F), specifying the region from which the final location is reachable in the remaining time slots. The region obtained by the intersection of two spheres $\mathcal{S}_P$ and $\mathcal{S}_F$ is now treated as the new feasible search region for that particular time slot which is denoted by $\mathcal{B}_m$ as shown in Fig. 4. Therefore, we limit the search space to $\mathcal{S}_P \bigcap \mathcal{S}_F$ instead of the entire sphere $\mathcal{S}_P$.

Thus, the effective solution to SP1 is reduced to solving a sequence of problems and finding the optimal location of the UAV in each time slot subjected to the feasible search region $\mathcal{B}_m$. Then, the effective problem that needs to be solved at mth-time slot is given by

$$\text{SP1a:} \max_{\{x^u[m], y^u[m], z^u[m]\}} \mathcal{R}_{\text{SP1}}[m] = \sum_{n=1}^{N} r_n[m]$$
$$\text{s.t.} \quad x^u[m], y^u[m], z^u[m] \in \mathcal{B}_m.$$

Problem SP1a is still nonconvex because the objective function is nonconvex. To solve this problem, we use alternating optimization while using convex approximation of the nonconcave function $r_n[m]$ in $x^u[m]$, $y^u[m]$, and $z^u[m]$.

C. Objective Reformulation in Problem SP1a

To deal with the nonconvexity in $x^u[m]$, $y^u[m]$, or $z^u[m]$, we approximate $r_n[m]$ to $\widetilde{r}_n[m]$. In particular, the nonconvexity in $r_n[m]$ arises due to the Sigmoidal function in (1). Therefore, we approximate the Sigmoidal function into a linear function [29], to get $\widetilde{r}_n[m]$ from $r_n[m]$ and is given as

Authorized licensed use limited to: Beijing Information Science & Tech Univ. Downloaded on March 19,2023 at 02:57:14 UTC from IEEE Xplore. Restrictions apply.

$$\widetilde{r}_n[m] = \frac{B}{N} \log_2\left(1 + \frac{\tilde{\gamma}_o\left(\frac{(1-\kappa)z^u[m]}{\sqrt{\left(x^u[m]-x_n^g\right)^2+\left(y^u[m]-y_n^g\right)^2+\left(z^u[m]\right)^2}}+\kappa\right)}{\left(\left(x^u[m]-x_n^g\right)^2+\left(y^u[m]-y_n^g\right)^2+\left(z^u[m]\right)^2\right)^{\alpha}}\right) \quad (15)$$

where $\alpha = \bar{\alpha}/2$ and $\tilde{\gamma}_o = P_{tr}\beta_0/\sigma^2$. Taking $\widetilde{r}_n[m]$ instead of $r_n[m]$ in problem SP1a is still a nonconvex problem, due to the fact that $\widetilde{r}_n[m]$ is neither convex nor concave in $x^u[m]$. However, it is convex in $(x^u[m]-x_n^g)^2$ and $(y^u[m]-y_n^g)^2$ (this result can be obtained by modifying [29, Lemma 2]), and according to [10], any convex function can be globally lower bounded by its first-order Taylor expansion at any point. Let $x^{u,j}[m]$ be the UAV location at jth-iteration, then the lower bound of $\widetilde{r}_n[m]$ is given by

$$\widetilde{r}_n[m] \geq \mathcal{A}_x[m] - \mathcal{D}_x[m]\frac{\left(\left(x^u[m]-x_n^g\right)^2-\left(x^{u,j}[m]-x_n^g\right)^2\right)}{\mathcal{C}_x[m]} \triangleq \widehat{r}_n^{x^u}[m] \quad (16)$$

where

$$\mathcal{A}_x[m] = \frac{B}{N}\log\left(1+\tilde{\gamma}_o\,\mathcal{C}_x[m]^{-\alpha}\left(\kappa - \frac{(\kappa-1)z^u[m]}{\sqrt{\mathcal{C}_x[m]}}\right)\right) \quad (17)$$

$$\mathcal{D}_x[m] = \frac{\frac{\tilde{\gamma}_o}{2}\frac{B}{N}\left(z^u[m](2\alpha\kappa-2\alpha+\kappa-1)-2\alpha\sqrt{\mathcal{C}_x[m]}\kappa\right)}{\mathcal{C}_x[m]\left(-\mathcal{C}_x[m]^{\alpha+\frac{1}{2}}-\sqrt{\mathcal{C}_x[m]}\tilde{\gamma}_o\kappa-\tilde{\gamma}_o(1-\kappa)z^u[m]\right)} \quad (18)$$

$$\mathcal{C}_x[m] = \left(x^{u,j}[m]-x_n^g\right)^2+\left(y^u[m]-y_n^g\right)^2+\left(z^u[m]\right)^2). \quad (19)$$

Also, by introducing the slack variable $s^{x^u}[m] = (x^u[m]-x_n^g)^2$, we have

$$s^{x^u}[m] \leq \left(x^{u,j}[m]-x_n^g\right)^2+2\left(x^{u,j}[m]-x_n^g\right)\left(x^u[m]-x^{u,j}\right) \leq \left(x^u[m]-x_n^g\right)^2. \quad (20)$$

Since the behavior of $y^u[m]$ in (15) is similar to $x^u[m]$. The same results can also be applied for $y^u[m]$. Accounting (20) and (16), problem SP1b to optimize $x^u[m]$, and $y^u[m]$ can be reformulated as follows:

$$\text{SP1b:} \max_{\varphi[m],s^{\varphi}[m]} \sum_{n=1}^{N}\widehat{r}_n^{\varphi}[m]$$

$$\text{s.t.} \quad \varphi[m] \in \mathcal{B}_m \quad (21a)$$

$$s^{\varphi}[m] \leq \left(\varphi^j[m]-x_n^g\right)^2+2\left(\varphi^j[m]-x_n^g\right)\left(\varphi[m]-\varphi^j[m]\right) \quad (21b)$$

where $\varphi[m] \in \{x^u, y^u\}$ and $\varphi^j \in \{x^{u,j}, y^{u,j}\}$. It can be verified that the problem in convex in φ and can be readily solved using the interior point method [10].

D. Algorithmic Implementation of Problem SP1

The objective function $\widetilde{r}_n[m]$ is a complicated function of $z^u[m]$ whose monotonicity as well as concavity is difficult to prove. According to [33], for a fixed value of $x^u[m]$ and $y^u[m]$, the objective function property as a function of $z^u[m]$ can be illustrated in a graph, shown in Fig. 5. We consider four scenarios and for each scenario, we observe that the sum throughput $\sum_{i=1}^{N} r_n[m]$ first increases with height and then decreases. As a result, there is only a single maxima in all these four scenarios. Therefore, we apply golden section search (GSS) [35] to obtain a optimal value of $z^u[m]$ in a time slot.

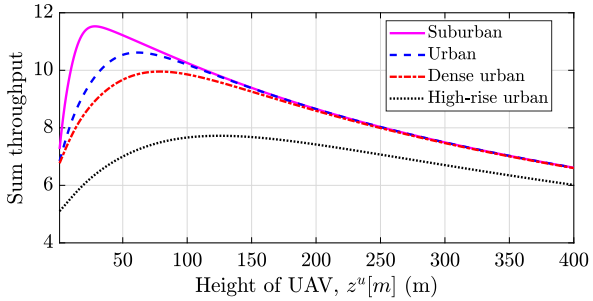

Fig. 5. Sum throughput versus height $z^u[m]$ for $x^u[m] = y^u[m] = -10$ m.

Algorithm 1 Effective Solution to SP1

Input: (x^I, y^I, z^I), (x^F, y^F, z^F), $H_{\min}$, $\tau[m]$, $v[m]$, N, (x_n^g, y_n^g), $\forall n \in \mathcal{N}$, and ϵ.

Output: $\mathcal{R}_{\text{SP1}}^{sum^*}$, $\mathcal{R}_{\text{SP1}}[m]^*$ along with $\mathcal{X}[m] = (x^u[m]^*, y^u[m]^*, z^u[m]^*)$.

for $m = 1 : M$ **do**
  Compute feasible search region $\mathcal{B}_m$.
  Initialize iteration number $l = 0$, maximum iteration $l^{\max}$. Initialize feasible solution $(x^u[m-1], y^u[m-1], z^u[m-1])$ and set $\mathcal{R}_{\text{SP1}}^0[m] = \mathcal{R}_{\text{SP1}}[m-1]$.
  repeat
  Obtain $x^{u,l+1}[m]$ using SP1b for fixed $(y^{u,l}[m], z^{u,l}[m])$.
  Obtain $y^{u,l+1}[m]$ using SP1b for fixed $(x^{u,l+1}[m], z^{u,l}[m])$.
  Obtain $z^{u,l+1}[m]$ using SP1a for fixed $(x^{u,l+1}[m], y^{u,l+1}[m])$.
  With $(x^{u,l+1}[m], y^{u,l+1}[m], z^{u,l+1}[m])$, calculate $\mathcal{R}_{\text{SP1}}^{l+1}[m]$.
  Update $l = l + 1$.
  Until $|\mathcal{R}_{\text{SP1}}^{l+1}[m] - \mathcal{R}_{\text{SP1}}^{l}[m]| < \epsilon$ or $l > l^{\max}$
  Set $\mathcal{R}_{\text{SP1}}[m]^* = \mathcal{R}_{\text{SP1}}^{l+1}[m]$.
end for
Set $\mathcal{R}_{\text{SP1}}^{sum^*} = \sum_{m=1}^{M}\mathcal{R}_{\text{SP1}}[m]^*$.

Based on subproblem SP1b to optimize $x^u[m]$ and $y^u[m]$, and SP1a to optimize $z^u[m]$, we present Algorithm 1 for solving SP1 based on alternating optimization, where the solution is based on optimizing the sequence of $x^u[m]^*$, $y^u[m]^*$, and $z^u[m]^*$. The detailed steps of Algorithm 1 are as follows: First, it computes the feasible search region $\mathcal{B}_m = \mathcal{S}_P \bigcap \mathcal{S}_F$ for the mth-time slot using geometric techniques. Second, for a given $\mathcal{B}_m$, it sets the initial iteration count l, and the maximum number of iteration count to $l^{\max}$. Then, at each iteration it optimizes the sequence of $x^u[m]^*$, $y^u[m]^*$, and $z^u[m]^*$. At each iteration l, the algorithm computes the sum throughput over all users at the mth-time slot denoted by $\mathcal{R}_{\text{SP1}}^{l+1}[m]$. For the mth-time slot, the search for optimal location is completed when $|\mathcal{R}_{\text{SP1}}^{l+1}[m] - \mathcal{R}_{\text{SP1}}^{l}[m]| < \epsilon$, where $\mathcal{R}_{\text{SP1}}^{l+1}[m]$ and $\mathcal{R}_{\text{SP1}}^{l}[m]$ is the sum throughput over all users at the $(l+1)$th and lth-iteration, respectively, and ϵ is the acceptable tolerance. It also stops when $l > l^{\max}$. This procedure is repeated for $m \leq M$ time slots until the UAV reaches the final location. Finally, the algorithm returns the UAV trajectory denoted by $\mathcal{X}[m]^* \triangleq (x^u[m]^*, y^u[m]^*, z^u[m]^*) \quad \forall m \in \mathcal{M}$, and the overall throughput given by $\mathcal{R}_{\text{SP1}}^{\text{sum}^*} = \sum_{m=1}^{M}\mathcal{R}_{\text{SP1}}[m]^*$, where $\mathcal{R}_{\text{SP1}}[m]^*$ is the sum throughput at the mth-time slot.

Authorized licensed use limited to: Beijing Information Science & Tech Univ. Downloaded on March 19,2023 at 02:57:14 UTC from IEEE Xplore. Restrictions apply.

E. Convergence of SP1

To ensure the convergence of the alternating optimization method for obtaining the solution to SP1, we show that in each iteration we are increasing the objective value in a maximization problem. In SP1a, to optimize $x^u[m]^*$ and $y^u[m]^*$, the problem is nonconvex, and to optimize $z^u[m]^*$, the function is unimodal. Therefore, we solve the approximate problem SP1b to optimally optimize $x^u[m]^*$ and $y^u[m]^*$.

Define $\mathcal{R}_x^{\dagger}(X, Y, Z) = \max_{x^u[m]} \mathcal{R}_{\text{SP1}}(X, Y, Z)$ as the maximum objective value of SP1b when optimizing over variable $x^u[m]$. Here, $X = x^u[m]$, $Y = y^u[m]$, and $Z = z^u[m]$. Also, let $\mathcal{R}_{\text{SP1}}(X^l, Y^l, Z^l)$ be the objective function value of the original subproblem SP1a, where X^l, Y^l, and Z^l are the values of X, Y, and Z at the lth-iteration, respectively. The following steps show how the objective function changes while optimizing variable $x^u[m]$:

$$\begin{aligned}\mathcal{R}_{\text{SP1}}\left(X^l, Y^l, Z^l\right) &\overset{(a)}{=} \mathcal{R}_x^{\dagger}\left(X^l, Y^l, Z^l\right)\\ &\overset{(b)}{\leq} \mathcal{R}_x^{\dagger}\left(X^{l+1}, Y^l, Z^l\right)\\ &\overset{(c)}{\leq} \mathcal{R}_{\text{SP1}}\left(X^{l+1}, Y^l, Z^l\right) \end{aligned} \tag{22}$$

where (a) holds because the first-order Taylor approximation defined in (16) is tight at the local point. This implies problem SP1b at X^l has the same objective value as that of problem SP1a. (b) holds since the problem is solved optimally to obtain X^{l+1} for a given Y^l and Z^l. Furthermore, (c) holds since the objective value of the approximate problem obtained by applying the first-order Taylor expansion is a lower bound on the original objective defined in SP1a. Thus, (22) implies that even though we have considered the approximate problem to obtain the solution, the objective function defined in SP1a is still nondecreasing at each iteration.

Next, in step 6 of Algorithm 1, optimization of Y^l for a given X^{l+1} and Z^l follows:

$$\mathcal{R}_{\text{SP1}}\left(X^{l+1}, Y^l, Z^l\right) \leq \mathcal{R}_{\text{SP1}}\left(X^{l+1}, Y^{l+1}, Z^l\right). \tag{23}$$

Similar explanation for (22) can be applied to (23). Since the third subproblem is unimodal, we apply GSS in step 7 of Algorithm 1 to optimize Z^l for a given value of X^{l+1}, and Y^{l+1}. Thus, we have

$$\mathcal{R}_{\text{SP1}}\left(X^{l+1}, Y^{l+1}, Z^l\right) \leq \mathcal{R}_{\text{SP1}}\left(X^{l+1}, Y^{l+1}, Z^{l+1}\right). \tag{24}$$

Based on (22)–(24), we obtain

$$\mathcal{R}_{\text{SP1}}\left(X^l, Y^l, Z^l\right) \leq \mathcal{R}_{\text{SP1}}\left(X^{l+1}, Y^{l+1}, Z^{l+1}\right). \tag{25}$$

This implies that the objective value is nondecreasing after each iteration of Algorithm 1. Algorithm 1 is guaranteed to converge as the objective function of problem SP1a is upper bounded by some finite value. Furthermore, since we have solved only the convex optimization problems (which are of polynomial complexity) in each iteration of Algorithm 1, Algorithm 1 can be easily implemented for faster convergence.

Remark 1: Note that the solution obtained using alternating optimization depends on the initial point from where the algorithm proceeds. To determine a suitable initial point, we consider a simple straight-line trajectory. The straight-line trajectory connecting the current and the final location is used to determine the initial UAV location in each time slot.

V. SP2: Velocity and Time Optimization

Taking into account the trajectory obtained from SP1, we construct subproblem SP2 that considers the acceleration constraints in (13e) of the UAV and provides the velocity-time profile of the UAV for the given trajectory obtained from SP1. The UAV position at different times is obtained by solving SP1 and is given as $\mathcal{X}[m]^* \triangleq (x^u[m]^*, y^u[m]^*, z^u[m]^*)$ and corresponding rates $\mathcal{R}_{\text{SP1}}[m]^*$ in the mth-slot. In this subproblem, the velocity and the slot duration in each time slot are optimized to obtain a velocity-time profile. Note that the UAV follows the same trajectory as obtained from SP1.

A. Mathematical Formulation

The idea here is to satisfy the time constraint in (13g) and acceleration constraint in (13e) by optimizing the time slot duration $\tau[m]$ and the velocity $v[m]$ of the UAV for all $m \in \mathcal{M}$ time slots. As we know from the kinematics equation defined in (10) and (11) that the acceleration in horizontal and vertical components is highly correlated to their respective velocity and the time slot duration. Thus, to optimize the acceleration of the UAV, we only need to optimize the velocity and the time slot duration of the UAV. From SP1, the distance traveled by the UAV in the mth-time slot is also known which is denoted by $d^s[m] \triangleq \|\mathcal{X}[m]^* - \mathcal{X}[m-1]^*\| \quad \forall m$, where $\mathcal{X}[m]^*$ and $\mathcal{X}[m-1]^*$ represent the optimal UAV locations. Thus, SP2 in terms of time slot duration and acceleration is formulated as follows:

$$\text{SP2:} \max_{v[m],\tau[m] \quad \forall m \in \mathcal{M}} \sum_{m=1}^{M} \tau[m]\mathcal{R}_{\text{SP1}}[m]^*$$

$$\text{s.t.} \quad v[m] - v[m-1] - A_{\max}\tau[m] \leq 0 \quad \forall m \in \mathcal{M} \tag{26a}$$

$$v[m] + v[m-1] - \frac{2d^s[m]}{\tau[m]} = 0 \quad \forall m \in \mathcal{M} \tag{26b}$$

$$v[0] = 0$$

$$(13e),\ (13g) \tag{26c}$$

where $\mathcal{R}_{\text{SP1}}[m]^*$ is obtained from SP1, i.e., sum throughput over all users at the mth-time slot. Equations (26a) and (26b) represent the constraints on the dynamics and kinematics of UAV that includes the constraint on acceleration and velocity. Equation (26c) states that the initial velocity is zero.

B. Algorithmic Implementation of Problem SP2

The solution to SP2 can be regarded as a feasible solution to (P1) when onboard energy availability constraint is relaxed. This is because of the following reasons.

1) The trajectory obtained from SP1 is a feasible solution of (P1) when acceleration and onboard energy availability constraints are relaxed because the UAV maximized the overall throughput of the system by following the maximum throughput locations in every time slot.
2) While following the optimal location, the UAV optimizes its time slot duration $\tau[m]$ and velocity $v[m]$ to

Authorized licensed use limited to: Beijing Information Science & Tech Univ. Downloaded on March 19,2023 at 02:57:14 UTC from IEEE Xplore. Restrictions apply.

Algorithm 2 Two-Stage Alternating Approach for SP2

Input: $\mathcal{R}_{\text{SP1}}[m]^*$.
Output: $\tau[m]^*$, $v[m]^*$, $\forall m \in \{1, \ldots, M\}$.
1: Set $l = 0$ and initialize $v[m]^l$.
2: **repeat**
3: With given $v[m]^l$ solve SP2 to obtain $\tau[m]^{l+1}$ by using (27) instead of (26b).
4: With given $\tau[m]^{l+1}$ solve SP2 to obtain $v[m]^{l+1}$.
5: Update $\tau[m]^{l+1} = \tau[m]^*$, $v[m]^{l+1} = v[m]^*$ and $l = l + 1$.
6: **Until** The objective function converges.

satisfy the constraints on time, maximum acceleration, and velocity. Thus, the solution obtained from SP2 is a feasible solution to (P1), when the energy availability constraint is relaxed.

Problem SP2 is difficult to solve directly due to the nonlinear constraint in (26a) and nonaffine constraint in (26b). To tackle this difficulty, a two-stage alternating optimization approach is proposed. In the first stage, the time slot duration $\tau[m]$ is optimized by fixing $v[m]$ obtained from SP1. Then, in the second stage, $v[m]$ is optimized for the obtained $\tau[m]$. The two stages are solved alternatively until the objective function defined in SP2 is below an acceptable threshold.

In the first stage, for the given $v[m]$, the constraint (26a) is a linear constraint and (26b) is a nonaffine constraint in $\tau[m]$. To tackle the nonaffine constraint, we apply SCA procedure at a feasible point $\tau[m]^l$ to make (26b) linear, where $\tau[m]^l$ denotes the value of $\tau[m]$ at the lth-iteration. Accounting this, (26b) can be rewritten as follows:

$$v[m]+v[m-1]-2d^s[m]\left(\frac{1}{\tau[m]^l}+\frac{\tau[m]-\tau[m]^l}{\left(\tau[m]^l\right)^2}\right)=0. \quad (27)$$

Using (27) in place of (26b) makes problem SP2 a linear programming problem in $\tau[m]$ for a given $v[m]$ which can be readily solved using the interior point method.

In the second stage, for a given $\tau[m]$ obtained from the first stage, it can be observed that problem SP2 is a linear programming problem in $v[m]$ since the constraint (26a) and (26b) are both linear in $v[m]$. Thus, the interior point method can be used to solve for $v[m]$ for a given $\tau[m]$.

Using the above discussion, the two-stage alternating approach to obtain the solution of SP2 is summarized in Algorithm 2. To start Algorithm 2, the initial velocity $v[m]$ for all time slots is set to the velocity of the UAV obtained from SP1. Thereafter, the algorithm optimizes $\tau[m]$ and $v[m]$ alternatively. The algorithm converges when the change in the objective function is below a predescribed threshold.

C. Convergence of SP2

Define $\mathcal{R}_{\text{SP2}}(\tau[m], v[m])$ as the value of objective function to the original problem SP2. Then at the lth-iteration, we have

$$\mathcal{R}_{\text{SP2}}\left(\tau[m]^l, v[m]^l\right) \le \mathcal{R}_{\text{SP2}}\left(\tau[m]^{l+1}, v[m]^l\right) \quad (28)$$

where (28) holds because the first-order Taylor expansion defined in (27) is tight at a local point, and the problem is solved optimally. Thus, (28) implies that the objective function defined in SP2 is nondecreasing after each iteration. Since the problem to optimize $v[m]$ is convex, then accordingly we have

$$\mathcal{R}_{\text{SP2}}\left(\tau[m]^{l+1}, v[m]^l\right) \le \mathcal{R}_{\text{SP2}}\left(\tau[m]^{l+1}, v[m]^{l+1}\right). \quad (29)$$

Based on (28) and (29), we observe that the objective value is nondecreasing after every iteration of Algorithm 2. Thus, Algorithm 2 is guaranteed to converge. Furthermore, only convex optimization problems are solved in each iteration of Algorithm 2. Thus, it can be effectively implemented with a faster convergence.

VI. Low-Complexity Iterative Approach

A. Implementation Details of Problem (P1)

As described in Fig. 3, the problem (P1) is decoupled into two subproblems and a feasibility check block. Here, we first solve the subproblems using the alternating optimization method and then iterate it depending upon the energy availability constraint. The feasibility check block checks the feasibility of the solution obtained by checking the overall energy consumed during the UAV's flight. Note that the velocity as a control parameter is used for SP1 such that the UAV trajectory changes when the solution iterates. This velocity is defined in constraint (14a) of SP1 as $v[m]$. This is chosen because we know from the energy model of a rotary-wing UAV that a higher UAV velocity corresponds to a higher energy consumption. Therefore, to decrease the total energy, we consider the velocity parameter to steer the solution of SP1.

The velocity $v[m]$ is updated whenever the energy consumption constraint is violated. This update (decrease) in velocity affects the trajectory, which becomes shorter on account of lower velocity. The proportional decrease in velocity can be related to the current energy consumption as

$$v[m]^i = \eta \times v[m]^{i-1} \quad (30)$$

where $\eta = (E_{\max}/\mathcal{E}_{\text{tot}})$, $v[m]^i$ is the updated velocity in the ith-iteration and $v[m]^{i-1}$ is the velocity in the previous iteration $(i-1)$.

With this explanation, we describe the solution of (P1) in Algorithm 3. The steps described in Algorithm 3 are as follows. First, at the beginning, we set $v[m] = V_{\max}$, then, problem SP1 is solved to obtain the UAV trajectory as described in Section IV-D. This solution is then passed to SP2 to optimize velocity, acceleration and time as described in Section V-B. Subproblems SP1 and SP2 are solved alternatively using the alternating optimization method to provide a converged solution. Thereafter, this solution is passed through the feasibility check block, where it checks the feasibility of solution in terms of onboard energy availability. The energy consumed by the UAV in a time slot is computed by decoupling the velocity and acceleration into its horizontal and vertical components as described in Section II-C and then it computes the total energy $\mathcal{E}_{\text{tot}}$ consumed during its flight. Lastly, if feasibility check block returns an infeasible solution (i.e., the onboard energy constraint is not satisfied), the proposed approach updates the velocity of SP1 ($v[m]$) as in (30) and calls SP1 again. This process is repeated until the solution obtained is feasible.

Authorized licensed use limited to: Beijing Information Science & Tech Univ. Downloaded on March 19,2023 at 02:57:14 UTC from IEEE Xplore. Restrictions apply.

Algorithm 3 Overall Algorithm to Obtain Solution of (P1)

Input: $(\mathrm{x^I}, \mathrm{y^I}, \mathrm{z^I})$, $(\mathrm{x^F}, \mathrm{y^F}, \mathrm{z^F})$, H_{min}, N, $(x_n^g, y_n^g), \forall n \in \mathcal{N}$, E_{max}, T_{max}, M, V_{max} and A_{max}.

1: Initialize $k = 0$, and set $v[m] = V_{max}$ and $\tau[m] = \frac{T_{\max}}{M}$.
2: Set $l = 0$, and initialize $\tau[m]^l$, $v[m]^l$.
3: **repeat**
4: Call Algorithm 1 to solve SP1 with $v[m]^l$ and $\tau[m]^l$.
5: Call Algorithm 2 to solve SP2 to obtain $v[m]^{l+1}$, $\tau[m]^{l+1}$.
6: Update $l = l + 1$.
7: **Until** Objective function converges
8: Calculate $v^{xy}[m]$, $v^z[m]$, $a^{xy}[m]$, and $a^z[m]$ using (8), (9), (10), and (11), respectively. Then, calculate $e^{xy}[m]$ and $e^z[m]$ defined in (6), and (7), respectively, to calculate $\mathcal{E}_{tot}$.
9: **repeat**
10: $k = k + 1$.
11: Calculate $v[m]^k$ using (30).
12: Repeat Steps 2-13.
13: **Until** $\mathcal{E}_{tot} < E_{\max}$

B. Complexity Analysis

The complexity of SP1 mainly depends upon steps 6–8 in Algorithm 1. Steps 6 and 7 are solved using the interior point method. According to [30], the complexity of solving a convex optimization problem using the interior point method is $\mathcal{O}(a^{0.5}(a+b)b^2)$, where a and b are the number of variables and the inequality constraints, respectively. To solve step 8 using GSS, the complexity is given by $\mathcal{O}(\lceil[\ln(\epsilon) - \ln(H_{\max} - H_{\min})]/\ln r\rceil)$ where ϵ is the acceptable error tolerance, $r \triangleq 0.618$ is the factor by which the search space reduces in each interval, and $H_{\max}$ can be regarded as the maximum height beyond which UAV is not allowed to fly [35]. Then, the overall complexity required to compute the solution to SP1 is given by $C_{\mathrm{SP1}} \triangleq \mathcal{O}(Ml^{\max}\max(2, \lceil[\ln(\epsilon) - \ln(H_{\max} - H_{\min})]/\ln 0.618\rceil))$.

SP2 is solved using alternating approach which involves transforming SP2 to a linear programming problem and then using the interior point method. Considering $M \gg 1$, the computations required to solve SP2 is given by $C_{\mathrm{SP2}} \triangleq \mathcal{O}(\max((M)^{2.5}(2M-1)))$.

The overall computations to solve (P1), i.e., Algorithm 3, lies in the number of iterations taken to obtain a feasible solution. Let $k_{\max}$ be the maximum iterations required to obtain a feasible solution. Then, the overall computations required to solve (P1) is given by $\mathcal{O}(k^{\max}\max(C_{\mathrm{SP1}}, C_{\mathrm{SP2}}))$.

C. Overall Convergence

To ensure the convergence of Algorithm 3, we first define $\mathcal{R}(T^l, \tau[m]^l, v[m]^l)$ as the objective value of the original problem, where $T = (x^u[m], y^u[m], z^u[m])$. The steps followed in Algorithm 3 is as follows. First, Algorithm 1 is executed to optimize $(x^u[m]^*, y^u[m]^*, z^u[m]^*)$ for a fixed $\tau[m]$ and $v[m]$. This follows:

$$\mathcal{R}\left(T^l, \tau[m]^l, v[m]^l\right) \leq \mathcal{R}\left(T^{l+1}, \tau[m]^l, v[m]^l\right) \quad (31)$$

from (25). Thereafter, Algorithm 2 is executed to optimize $\tau[m]$ and $v[m]$ for the given trajectory T^l. This implies

$$\mathcal{R}\left(T^{l+1}, \tau[m]^l, v[m]^l\right) \leq \mathcal{R}\left(T^{l+1}, \tau[m]^{l+1}, v[m]^{l+1}\right) \quad (32)$$

which follows from (28) and (29). Thereafter, we obtain

$$\mathcal{R}\left(T^l, \tau[m]^l, v[m]^l\right) \leq \mathcal{R}\left(T^{l+1}, \tau[m]^{l+1}, v[m]^{l+1}\right). \quad (33)$$

This implies objective value in every iteration of SP1 and SP2 increases and therefore Algorithm 3 is guaranteed to converge.

VII. Numerical Results and Discussion

From a system perspective, we consider a set of $N = 10$ GDs located randomly in a circular field of radius $r = 120$ m. The initial (x^I, y^I, z^I) and final (x^F, y^F, z^F) location of the UAV is set to $(-150, 0, 0)$ m and $(-1, 0, 36)$ m, respectively. In our work, we have considered the final location as the optimal location in 3-D space where the sum throughput over all users is maximum. This is carried out by following the procedure as defined in [36]. However, in general, the final location could be anything depending upon the geographical limitations or any other constraint. The minimum height $H_{\min}$ to be attained by the UAV before making lateral movement is set to 15 m. The total flight of the UAV is taken to be $T_{\max} = 20$ s, which is discretized in $M = 80$ slots. The environment parameters are taken as $C = 10$ and $D = 0.6$ [6]. The channel parameters, such as the ratio of $P_{tr}\beta_0/\sigma^2$ is set to 80 dB, pathloss exponent is set to $\alpha = 2.3$, and the additional attenuation factor is $\kappa = 0.2$ [6]. The total bandwidth B available for communication is set to 20 MHz. The simulation parameters taken for the energy consumption model of a rotary-wing UAV are given in Table II (Section II-C) [7].

A. Suboptimal Design Insights

In this section, we provide insight on the UAV 3-D trajectory and show how the velocity, acceleration, and trajectory vary with the change in the onboard energy availability $E_{\max}$. We set the maximum velocity $V_{\max}$ to 28 m/s and acceleration $A_{\max}$ to 10 m/s^2 [22].

To gain trajectory insights, we considered four cases. Case 1: $E_{\max}$ is set to 5.9 kilo-Joule (kJ) and Case 2: $E_{\max}$ is set to 5.6 kJ. This $E_{\max}$ is chosen such that the proposed approach requires multiple iterations of SP1 to provide a feasible solution. This implies the UAV velocity of SP1 is decreased from $V_{\max}$ in both the cases and thus the UAV takes more time to reach the final location. In cases 3 and 4, $E_{\max}$ is set to 5.3 and 5.0 kJ, respectively, in a way similar to case 2, but here the UAV velocity in SP1 is much lesser and the UAV takes full $T_{\max}$ time to reach the final location.

Fig. 6 presents the UAV trajectory obtained using our proposed scheme for the above-discussed cases. For $E_{\max} =$ 5.9 kJ, the UAV takes approximately 14.85 s to reach the final location, and the rest of the time is used to hover at the final location. However, when the energy is decreased to 5.6 kJ, the UAV velocity-time profile changes, the UAV moves slowly, and now takes 18.15 s to reach the final location. Though the trajectory remains the same. Finally, with even lesser energy (i.e., cases 3 and 4), the UAV consumes full $T_{\max} = 20$ s to reach the final location. As a result, no time is left for the UAV to hover at the final location.

To see the variation in velocity by which the UAV moves with respect to different $E_{\max}$, we plot Fig. 7(a). The velocity

Authorized licensed use limited to: Beijing Information Science & Tech Univ. Downloaded on March 19,2023 at 02:57:14 UTC from IEEE Xplore. Restrictions apply.

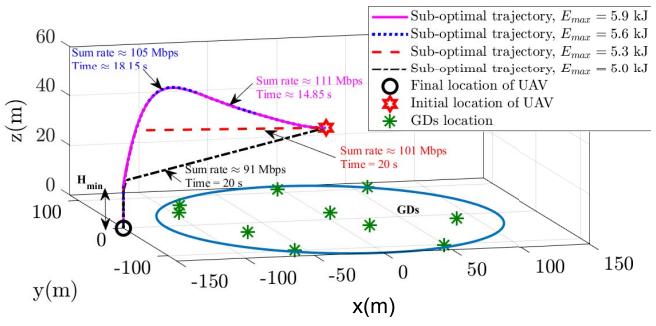

Fig. 6. Insights on 3-D UAV trajectory for the proposed scheme with different onboard energy availability $E_{\max}$.

profile shows that to maximize the system's performance, the UAV always moves with maximum velocity. This is because the final location is the optimal deployment location where the sum throughput over all GDs is maximum. In such a case, high throughput is ensured when the UAV spends more time at locations where the sum throughput is high. Thus, the UAV travels with the fixed velocity to attain a higher sum throughput. Also, it can be observed that for all energy levels, the UAV first increases its velocity, accounting for the acceleration constraint, and later de-accelerates to reach the final location.

Similarly, the acceleration plot in Fig. 7(b) shows the acceleration profile of the obtained UAV trajectory. It can be seen that the accelerating or de-accelerating peaks are obtained when the UAV attains the maximum velocity from zero velocity or decreases from maximum velocity to zero velocity at the final location. The left to right shift in peak is observed when the energy available with the UAV is decreased. This is because the UAV moves with a lower velocity and takes more time to reach the final location. A similar explanation can also be applied to the time slot duration $\tau[m]$ plot shown in Fig. 7(c). The duration of time slot $\tau[m]$ depends strictly upon the total time available with the UAV, i.e., $T_{\max}$. However, the trend of time slot duration is similar to the acceleration and velocity profile of the UAV for a given energy availability, since they are related as seen from (26a). Since energy consumed in a time slot is a function of the duration of time slot and velocity-acceleration profile, when a peak occurs in Fig. 7(b) and (c), the UAV also consumes high energy.

B. Performance Comparison

We consider the benchmark fly-and-hover scheme, proposed in [23], for comparison. In the fly-and-hover scheme, the UAV hovers over the individual user's location before reaching the final location. This scheme first computes the optimal sequence of users to be visited such that it maximizes the sum rate of the system. Thereafter, it obtains the UAV trajectory by considering velocity, acceleration, energy, and time constraints. In this scheme, the UAV is allowed to fly at a fixed height z^F. Apart from the fly-and-hover scheme, to the best of the author's knowledge, none of the prior works have optimized velocity-acceleration and trajectory jointly. Nevertheless, we have considered two additional conventional schemes, namely, straight flight trajectory [37] and inverted-L shaped trajectory [29] for comparison. In a straight flight trajectory, the UAV moves in a straight-line path to reach the final location. In an inverted-L shaped trajectory, the UAV first attains the height equal to z^F and then travels horizontally to reach the final location. In these schemes, the UAV accelerates with $A_{\max}$ to reach $V_{\max}$ and thereafter moves with a constant velocity $V_{\max}$. Finally, it de-accelerates to reach the final location with v[M] = 0. The energy constraint is satisfied by decreasing the maximum velocity of the UAV proportionately.

To show the improvement in sum throughput with the variation in the total onboard energy availability $E_{\max}$, we plot Fig. 8(a). It is observed that the proposed scheme performs better than the other benchmark schemes due to its ability to optimize velocity and time slot duration in every time slot to maximize the sum throughput. However, in the benchmark schemes, the trajectory is obtained by keeping the time slot duration fixed. In Fig. 8(a), the red star in the benchmark schemes show the minimal energy that must be available with the UAV to reach the final location. Below this energy threshold, the benchmark schemes return an infeasible solution. On the contrary, our proposed approach jointly optimizes velocity, acceleration, time, and trajectory providing service at lower energy levels. As the total energy availability increases, the UAV travels with a higher velocity and provides a higher sum rate. At higher $E_{\max}$, the sum rate becomes almost constant due to the UAV's inability to fly at speeds higher than the maximum permissible velocity limits.

In Fig. 8(b) and (c), the comparison of sum throughput based on $V_{\max}$ and $A_{\max}$, respectively, is shown. Fig. 8(b) is plotted when $A_{\max}$ is fixed to 10 m/s^2, while Fig. 8(c) is plotted when $V_{\max}$ is set to 28 m/s and in both the figures, $E_{\max}$ is set to 7.1 kJ. It is observed that as we increase the maximum velocity $V_{\max}$, the sum throughput increases because the UAV reaches the final location early. On the other hand, the acceleration constraint $A_{\max}$ limits the rate of change in velocity of UAV. Hence, time consumed to attain maximum velocity increases with decrease in $A_{\max}$ leading to a lower sum rate. Consequently, it can be concluded from the above results that our proposed scheme provides a significant improvement over the benchmark schemes and the maximum permissible velocity, acceleration, onboard energy, and time plays an essential role in designing the UAV dynamics.

C. Computational Complexity Comparison

To exhibit the computational complexity of our proposed scheme, we compute the actual execution time and compare it with the existing benchmark, i.e., the fly-and-hover scheme [23]. Table III presents the execution time for different schemes, measured on an Intel Core i7 processor with a CPU clock speed of 3.20 GHz. It can be clearly observed that the execution time of the proposed scheme is quite less in comparison to the fly-and-hover scheme. For brute force, when we consider $M = 3$, the execution time of brute force is 39 s, whereas, for the proposed scheme, it is 1.7 s. Even though brute force can provide the globally optimal solution, it is unable to handle large-scale deployments (i.e., for larger M) due to its overwhelming high computation time.

Authorized licensed use limited to: Beijing Information Science & Tech Univ. Downloaded on March 19,2023 at 02:57:14 UTC from IEEE Xplore. Restrictions apply.

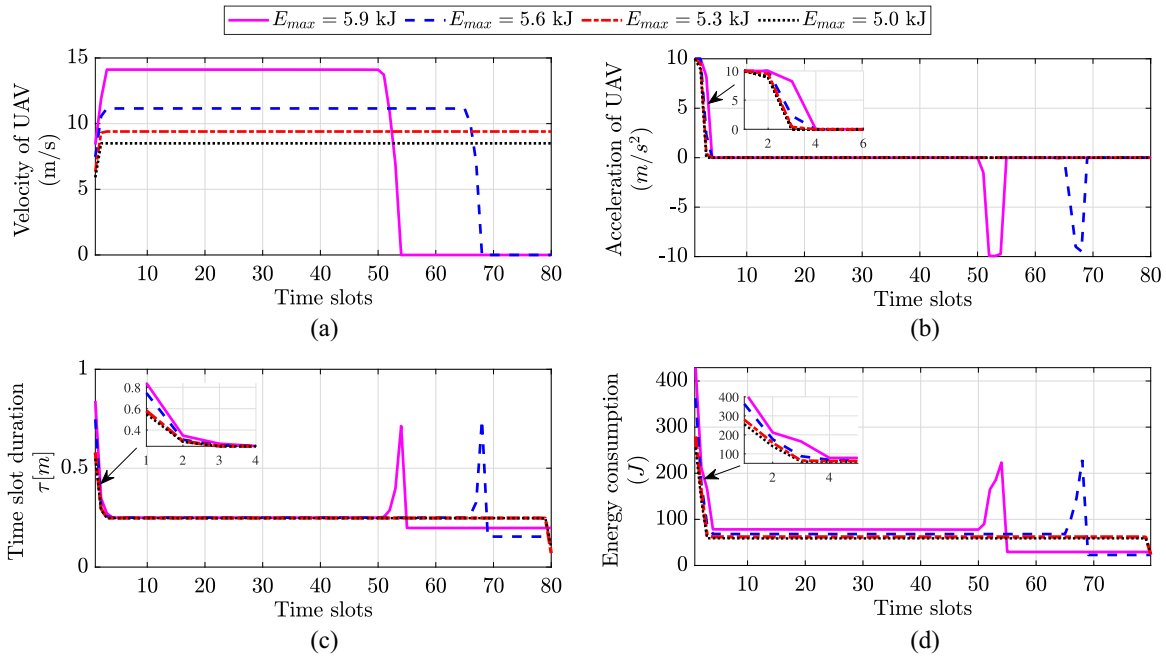

Fig. 7. Impact of onboard energy availability $E_{\max}$ on (a) velocity profile, (b) acceleration profile, (c) time slot duration, and (d) energy consumed per time slot.

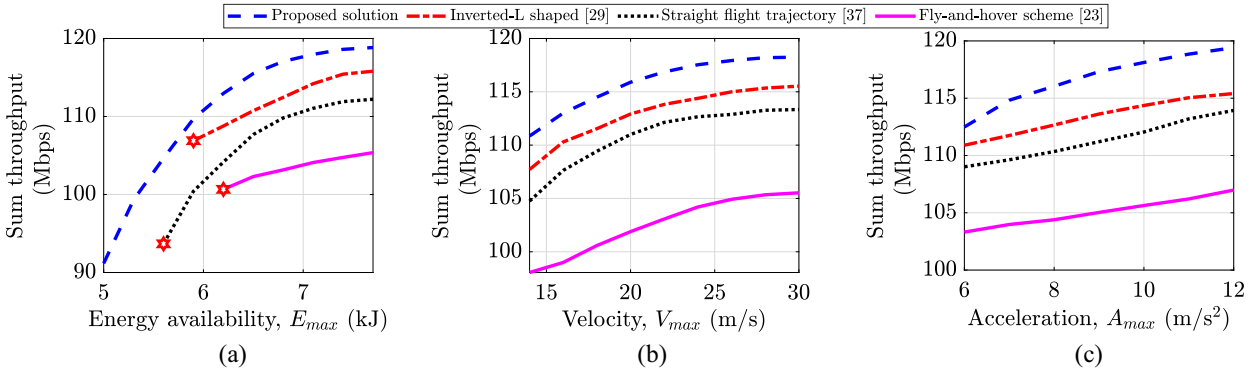

Fig. 8. Performance comparison of sum throughput of the proposed scheme with existing benchmark schemes by varying (a) $E_{\max}$, (b) $V_{\max}$, and (c) $A_{\max}$.

TABLE III
EXECUTION TIME (IN SECONDS) FOR DIFFERENT APPROACHES

	Energy availability, E_{max} (kJ)					
	5	5.5	6	6.5	7	7.5
Proposed approach	36	25.5	21.2	18.4	14.3	12.1
Fly-and-hover	44.5	37.3	30.1	25.3	19.7	16.2

VIII. CONCLUSION

In this article, a UAV-enabled IoT communication system is studied, where a rotary-wing UAV is dispatched from the initial to the final location to serve the GDs. To show the effective communication, we consider a system-centric performance metric with sum throughput as the objective parameter. To maximize the objective, we jointly optimize the 3-D trajectory and velocity-time profile in the presence of an accurate energy consumption model. The problem framed is nonconvex and it is difficult to obtain a globally optimal solution. Therefore, we propose a low-complexity solution that utilizes alternating optimization to obtain the 3-D trajectory and velocity-time profile. Simulation results show the effectiveness of the proposed approach over the benchmark schemes.

REFERENCES

[1] Q. Wu *et al.*, "Cognitive Internet of Things: A new paradigm beyond connection," *IEEE Internet Things J.*, vol. 1, no. 2, pp. 129–143, Apr. 2014.

[2] F. Javed, M. K. Afzal, M. Sharif, and B.-S. Kim, "Internet of Things (IoT) operating systems support, networking technologies, applications, and challenges: A comparative review," *IEEE Commun. Surveys Tuts.*, vol. 20, no. 3, pp. 2062–2100, 3rd Quart., 2018.

[3] N. Gupta, D. Mishra, and S. Agarwal, "Energy-aware trajectory design for outage minimization in UAV-assisted communication systems," *IEEE Trans. Green Commun. Netw.*, early access, Jan. 26, 2022, doi: 10.1109/TGCN.2022.3146627.

[4] M. Mozaffari, W. Saad, M. Bennis, Y. Nam, and M. Debbah, "A tutorial on UAVs for wireless networks: Applications, challenges, and open problems," *IEEE Commun. Surveys Tuts.*, vol. 21, no. 3, pp. 2334–2360, 3rd Quart., 2019.

[5] A. Girdher, A. Bansal, and A. Dubey, "Second-order statistics for IRS-assisted multiuser vehicular network with co-channel interference," *IEEE Trans. Intell. Veh.*, early access, May 12, 2022, doi: 10.1109/TIV.2022.3174641.

Authorized licensed use limited to: Beijing Information Science & Tech Univ. Downloaded on March 19,2023 at 02:57:14 UTC from IEEE Xplore. Restrictions apply.

[6] Y. Zeng, J. Xu, and R. Zhang, "Energy minimization for wireless communication with rotary-wing UAV," *IEEE Trans. Wireless Commun.*, vol. 18, no. 4, pp. 2329–2345, Apr. 2019.
[7] Z. Yang, W. Xu, and M. Shikh-Bahaei, "Energy efficient UAV communication with energy harvesting," *IEEE Trans. Veh. Technol.*, vol. 69, no. 2, pp. 1913–1927, Feb. 2020.
[8] Z. Xue, J. Wang, G. Ding, H. Zhou, and Q. Wu, "Maximization of data dissemination in UAV-supported Internet of Things," *IEEE Wireless Commun. Lett.*, vol. 8, no. 1, pp. 185–188, Feb. 2019.
[9] Q. Wu, Y. Zeng, and R. Zhang, "Joint trajectory and communication design for multi-UAV enabled wireless networks," *IEEE Trans. Wireless Commun.*, vol. 17, no. 3, pp. 2109–2121, Mar. 2018.
[10] Y. Zeng, R. Zhang, and T. J. Lim, "Throughput maximization for UAV-enabled mobile relaying systems," *IEEE Trans. Commun.*, vol. 64, no. 12, pp. 4983–4996, Dec. 2016.
[11] C. You and R. Zhang, "Hybrid offline-online design for UAV-enabled data harvesting in probabilistic LoS channels," *IEEE Trans. Wireless Commun.*, vol. 19, no. 6, pp. 3753–3768, Jun. 2020.
[12] C. You and R. Zhang, "3D trajectory optimization in Rician fading for UAV-enabled data harvesting," *IEEE Trans. Wireless Commun.*, vol. 18, no. 6, pp. 3192–3207, Jun. 2019.
[13] W. Lu *et al.*, "Resource and trajectory optimization for secure communications in dual unmanned aerial vehicle mobile edge computing systems," *IEEE Trans. Ind. Informat.*, vol. 18, no. 4, pp. 2704–2713, Apr. 2022.
[14] Y. Sun, D. Xu, D. W. K. Ng, L. Dai, and R. Schober, "Optimal 3D-trajectory design and resource allocation for solar-powered UAV communication systems," *IEEE Trans. Commun.*, vol. 67, no. 6, pp. 4281–4298, Jun. 2019.
[15] Q. Wu, Y. Zeng, and R. Zhang, "Joint trajectory and communication design for UAV-enabled multiple access," in *Proc. IEEE Global Commun. Conf. (GLOBECOM)*, Dec. 2017, pp. 1–6.
[16] M. Hua, L. Yang, C. Pan, and A. Nallanathan, "Throughput maximization for full-duplex UAV aided small cell wireless systems," *IEEE Wireless Commun. Lett.*, vol. 9, no. 4, pp. 475–479, Apr. 2020.
[17] Y. Liu, K. Xiong, Q. Ni, P. Fan, and K. B. Letaief, "UAV-assisted wireless powered cooperative mobile edge computing: Joint offloading, CPU control, and trajectory optimization," *IEEE Internet Things J.*, vol. 7, no. 4, pp. 2777–2790, Apr. 2020.
[18] S. Zhang, H. Zhang, B. Di, and L. Song, "Joint trajectory and power optimization for UAV sensing over cellular networks," *IEEE Commun. Lett.*, vol. 22, no. 11, pp. 2382–2385, Nov. 2018.
[19] S. Ahmed, M. Z. Chowdhury, S. R. Sabuj, M. I. Alam, and Y. M. Jang, "Energy-efficient UAV relaying robust resource allocation in uncertain adversarial networks," *IEEE Access*, vol. 9, pp. 59920–59934, 2021.
[20] L. Xiao, Y. Xu, D. Yang, and Y. Zeng, "Secrecy energy efficiency maximization for UAV-enabled mobile relaying," *IEEE Trans. Green Commun. Netw.*, vol. 4, no. 1, pp. 180–193, Mar. 2020.
[21] S. Ahmed, M. Z. Chowdhury, and Y. M. Jang, "Energy-efficient UAV relaying communications to serve ground nodes," *IEEE Commun. Lett.*, vol. 24, no. 4, pp. 849–852, Apr. 2020.
[22] H. Yan, Y. Chen, and S.-H. Yang, "New energy consumption model for rotary-wing UAV propulsion," *IEEE Wireless Commun. Lett.*, vol. 10, no. 9, pp. 2009–2012, Sep. 2021.
[23] M. T. Nguyen and L. B. Le, "Flight scheduling and trajectory control in UAV-based wireless networks," in *Proc. IEEE Wireless Commun. Netw. Conf. (WCNC)*, May 2020, pp. 1–6.
[24] S. Eom, H. Lee, J. Park, and I. Lee, "UAV-aided wireless communication designs with propulsion energy limitations," *IEEE Trans Veh. Technol.*, vol. 69, no. 1, pp. 651–662, Jan. 2020.
[25] X. Jing, J. Sun, and C. Masouros, "Energy aware trajectory optimization for aerial base stations," *IEEE Trans. Commun.*, vol. 69, no. 5, pp. 3352–3366, May 2021.
[26] Q. Hu, Y. Cai, A. Liu, G. Yu, and G. Y. Li, "Low-complexity joint resource allocation and trajectory design for UAV-aided relay networks with the segmented ray-tracing channel model," *IEEE Trans. Wireless Commun.*, vol. 19, no. 9, pp. 6179–6195, Sep. 2020.
[27] T. Zhang, J. Lei, Y. Liu, C. Feng, and A. Nallanathan, "Trajectory optimization for UAV emergency communication with limited user equipment energy: A safe-DQN approach," *IEEE Trans. Green Commun. Netw.*, vol. 5, no. 3, pp. 1236–1247, Sep. 2021.
[28] Z. Wu, Z. Yang, C. Yang, J. Lin, Y. Liu, and X. Chen, "Joint deployment and trajectory optimization in UAV-assisted vehicular edge computing networks," *J. Commun. Netw.*, vol. 24, no. 1, pp. 47–58, Feb. 2022.
[29] N. Gupta, S. Agarwal, and D. Mishra, "Trajectory design for throughput maximization in UAV-assisted communication system," *IEEE Trans. Green Commun. Netw.*, vol. 5, no. 3, pp. 1319–1332, Sep. 2021.
[30] A. Meng, X. Gao, Y. Zhao, and Z. Yang, "3D trajectory optimization for energy-constrained UAV-enabled IoT system in probabilistic LoS channel," *IEEE Internet Things J.*, vol. 9, no. 2, pp. 1109–1121, Jan. 2022.
[31] X. Xu, Y. Zeng, Y. L. Guan, and R. Zhang, "Overcoming endurance issue: UAV-enabled communications with proactive caching," *IEEE J. Sel. Areas Commun.*, vol. 36, no. 6, pp. 1231–1244, Jun. 2018.
[32] T. Zhang, G. Liu, H. Zhang, W. Kang, G. K. Karagiannidis, and A. Nallanathan, "Energy-efficient resource allocation and trajectory design for UAV relaying systems," *IEEE Trans. Commun.*, vol. 68, no. 10, pp. 6483–6498, Oct. 2020.
[33] R. I. Bor-Yaliniz, A. El-Keyi, and H. Yanikomeroglu, "Efficient 3D placement of an aerial base station in next generation cellular networks," in *Proc. IEEE Int. Conf. Commun. (ICC)*, Kuala Lumpur, Malaysia, May 2016, pp. 1–5.
[34] Y. Zeng and R. Zhang, "Energy-efficient UAV communication with trajectory optimization," *IEEE Trans. Wireless Commun.*, vol. 16, no. 6, pp. 3747–3760, Jun. 2017.
[35] Y.-C. Chang, "N-dimension golden section search: Its variants and limitations," in *Proc. BMEI*, Tianjin, China, Oct. 2009, pp. 1–6.
[36] N. Gupta, S. Agarwal, and D. Mishra, "UAV deployment for throughput maximization in a UAV-assisted cellular communications," in *Proc. IEEE 32nd Annu. Int. Symp. Pers. Indoor Mobile Radio Commun. (PIMRC)*, Helsinki, Finland, Sep. 2021, pp. 1055–1060.
[37] C. Zhan, Y. Zeng, and R. Zhang, "Energy-efficient data collection in UAV enabled wireless sensor network," *Wireless Commun. Lett.*, vol. 7, no. 3, pp. 328–331, Jun. 2018.

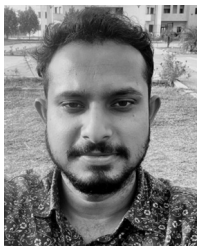

Nishant Gupta (Student Member, IEEE) received the B.Tech. degree in electronics and communication engineering from Chandigarh Engineering College, Mohali, India, in 2015, and the M.Tech. degree in electronics and communication from Panjab University, Chandigarh, India, in 2018. He is currently pursuing the Ph.D. degree with the Department of Electrical Engineering, Indian Institute of Technology Ropar, Rupnagar, India.

His research interests include 5G networks, UAV communications, and optimization.

Satyam Agarwal (Member, IEEE) received the Ph.D. degree in electrical engineering from IIT Delhi, New Delhi, India, in 2016.

He is currently an Assistant Professor with the Department of Electrical Engineering, IIT Ropar, Rupnagar, India. Prior to this, he was an Assistant Professor with IIT Guwahati, Guwahati, India. In 2017, he was a Postdoctoral Researcher with the Politecnico di Torino, Turin, Italy. His research interests are in the wide areas of wireless communication networks, including next-generation networks, 5G networks and architecture, and airborne networks.

Deepak Mishra (Member, IEEE) received the B.Tech. degree in electronics and communication engineering from Guru Gobind Singh Indraprastha University, New Delhi, India, in 2012, and the Ph.D. degree in electrical engineering from the Indian Institutes of Technology Delhi, New Delhi, in 2017.

He has been a Senior Research Associate with the School of Electrical Engineering and Telecommunications, University of New South Wales Sydney, NSW, Australia, since August 2019. His current research interests include wireless sensing systems, energy harvesting cooperative communication networks, massive MIMO, backscattering, physical-layer security, as well as signal processing and energy optimization schemes for the uninterrupted operation of wireless networks.

Authorized licensed use limited to: Beijing Information Science & Tech Univ. Downloaded on March 19,2023 at 02:57:14 UTC from IEEE Xplore. Restrictions apply.